AGU ADVANCING EARTH AND SPACE SCIENCES

Geophysical Research Letters

RESEARCH LETTER
10.1029/2025GL115600

Disruption of Drought Teleconnections Between ENSO-Influenced Regions Around 1700 CE

Max C. A. Torbenson[1], David W. Stahle[2], Edward R. Cook[3], Benjamin I. Cook[3,4], Ulf Büntgen[5,6,7], Feng Chen[8,9], Ernesto Tejedor[10], James H. Stagge[11], Miroslav Trnka[6,12], Dorian J. Burnette[13], Weipeng Yue[8], and Jan Esper[1,6]

[1]Department of Geography, Johannes Gutenberg Universität, Mainz, Germany, [2]Department of Geoscience, University of Arkansas, Fayetteville, AR, USA, [3]Lamont-Doherty Earth Observatory, Columbia University, New York, NY, USA, [4]NASA Goddard Institute for Space Studies, New York, NY, USA, [5]Department of Geography, University of Cambridge, Cambridge, UK, [6]Global Change Research Institute of the Czech Academy of Sciences, Brno, Czech Republic, [7]Department of Geography, Masaryk University, Brno, Czech Republic, [8]Institute of International Rivers and Eco-Security, Yunnan University, Kunming, China, [9]Institute of Desert Meteorology, Chinese Meteorological Administration, Urumqi, China, [10]Department of Geology, National Museum of Natural Sciences – Spanish Research Council, Madrid, Spain, [11]Department of Civil, Environmental and Geodetic Engineering, Ohio State University, Columbus, OH, USA, [12]Department of Agrosystems and Bioclimatology, Mendel University in Brno, Brno, Czech Republic, [13]Department of Earth Sciences, University of Memphis, Memphis, TN, USA

Key Points:

- Drought estimates based on tree rings in four El Niño Southern Oscillation (ENSO)-influenced regions become disconnected in the early 17th century CE
- Data assimilation and climate model outputs fail to capture a disruption of similar magnitude
- Future ENSO-driven drought teleconnections may include previously unknown variability

Supporting Information:

Supporting Information may be found in the online version of this article.

Correspondence to:

M. C. A. Torbenson,
mtorbens@uni-mainz.de

Citation:

Torbenson, M. C. A., Stahle, D. W., Cook, E. R., Cook, B. I., Büntgen, U., Chen, F., et al. (2025). Disruption of drought teleconnections between ENSO-influenced regions around 1700 CE. *Geophysical Research Letters*, *52*, e2025GL115600. https://doi.org/10.1029/2025GL115600

Received 28 FEB 2025
Accepted 26 JUN 2025

Abstract Our understanding of pre-modern El Niño Southern Oscillation (ENSO) variability is reliant on proxy records, often distant from the center of ENSO activity in the equatorial Pacific Ocean. Here, we assess the relationship between reconstructed soil moisture in four distant ENSO-influenced regions over the past 400 years. A major breakdown in the teleconnection of regional drought conditions in Asia, Eastern Australia, and North America is identified around 1700 CE. The statistically significant decline in inter-series correlations ($p < 0.01$) represents a previously unknown aspect of global hydroclimate dynamics. We hypothesize that the disruption was driven by ENSO weakening and/or by a large-scale multi-decadal reconfiguration of ocean-atmosphere circulation. Data assimilation estimates of soil moisture from the same regions fail to produce results of the same magnitude, potentially due to an overreliance of ENSO influence on the boundaries of spatial covariance in the underlying climate models.

Plain Language Summary The El Niño Southern Oscillation (ENSO) is a recurring change in sea surface temperatures in the tropical Pacific Ocean that affects climate across much of the globe. ENSO can influence drought conditions on land, all around the Pacific Ocean and beyond. Here, we use tree-ring estimates of drought to see how coherent dryness and wetness in these regions have been over the past 400 years. Overall, the four regions we study are in agreement but there is a breakdown in the relationship around 1700 CE. During this period, drought conditions in inner Eurasia, eastern Australia, southeast Asia, and southwest North America were unconnected. Climate models for the past millennium highlight how rare such an event is. The breakdown in drought teleconnection we describe may represent an important component of ENSO that so far is not fully understood.

1. Introduction

The El Niño Southern Oscillation (ENSO) is one of the strongest drivers of interannual climate variability at the global scale (Sarachik & Cane, 2010). Warm (El Niño) and cold (La Niña) sea surface conditions in the equatorial Pacific not only orchestrate precipitation and temperature over large parts of the Americas (Cai et al., 2020; Stagge et al., 2023), southeastern Asia (Nguyen-Thanh et al., 2023), and Australasia (Liguori et al., 2022), but also beyond the Pacific Ocean (Cai et al., 2018; Yeh et al., 2018), including the Horn of Africa (Gebre et al., 2023) and southern Africa (Meque & Abiodun, 2015). Considerable consequences of ENSO-related weather extremes on society have been described for many regions (IPCC, 2021; McGregor & Ebi, 2018).

The magnitude of ENSO influences is evident in global mean temperatures, with El Niño years appearing as extreme anomalies superimposed to the recent anthropogenic warming trend (Esper et al., 2024; Raghuraman et al., 2024). Global warming may in itself also influence the oscillation (Cai et al., 2015; Yeh et al., 2018). It has been suggested that recent decades have experienced an increase in ENSO variability (Cai et al., 2021), but output

from climate models show varying degrees of change to ENSO, with little inter-model agreement (Heede & Fedorov, 2023; Yeh et al., 2018). Although changes in teleconnections driven by ENSO may be even more difficult to predict (Cai et al., 2018), it has been argued that inter-regional drought may worsen (Singh et al., 2022). Regardless, the future state of ENSO-climate relationships will have considerable impact on how societies prepare to adapt or mitigate to associated climate conditions.

As studies explore the state of future ENSO variability and its teleconnection with regional hydroclimate, it is apparent that additional information regarding past behavior will benefit our knowledge on this complex ocean-atmospheric coupling (Scroxton & McKay, 2024; Wittenberg, 2009). Proxy records have been highlighted as a key source for understanding long-term ENSO variability and stability (Rosenthal & Broccoli, 2004). However, only a few proxy records with annual resolution and absolute dating precision exist for the Pacific Ocean and reflect direct ENSO signals. One major exception is the isotopic composition of living and subfossil corals that have been collected from various atolls, including Tarawa (Cole et al., 1993) and Palmyra (Cobb et al., 2001). Although reconstructions have been produced (e.g., Cobb et al., 2003; Freund et al., 2019), such records are rare and may further be limited by issues of replication, temporal coverage, and resolution (Tierney et al., 2015).

Proxy records from ENSO teleconnection regions are more plentiful and exploratory reconstructions based on tree-ring chronologies have been produced since the 1980s (D'Arrigo et al., 2005; Lough & Fritts 1985; Stahle & Cleaveland, 1993; Stahle et al., 1998). More recently, networks of tree-ring chronologies covering the larger Pacific Ocean region (Cook & Cane, 2024; Li et al., 2013), as well as multi-proxy data sets (Liu et al., 2024), have been used to estimate past changes in ENSO. Similarly, pre-instrumental ENSO estimates are available in data assimilation products that combine proxy data and model simulations (Luo et al., 2024; Zhu et al., 2022). The relationship between ENSO and remote climate variability is, however, likely non-linear (An & Jin, 2004; Tang et al., 2024) and unstable over space and time (Cole & Cook, 1998). The stability of the ENSO imprint on tree-ring chronologies may likewise fluctuate in time and space (Torbenson et al., 2019). Such changes can influence the robustness of past ENSO estimates that rely on proxies from teleconnection regions (Wilson et al., 2009).

Here, we assess the temporal stability of drought agreement between four regions of strong ENSO-influence: Inner Eurasia, Southeast Asia, Eastern Australia, and the TexMex region of North America. Regional soil moisture averages from tree ring-based reconstructions are compared from 1600 CE to present. Relative changes in correlation between regional pairs of past conditions are quantified throughout the past four centuries, and model-driven estimates of the same hydroclimatic variables are further explored for comparison.

2. Data and Methods

2.1. ENSO Index and Instrumental Climate Data

The extended multivariate ENSO index (eMEI; Wolter & Timlin, 2011), available from 1871 CE, was used to assess ENSO influence on large-scale drought conditions derived from the self-calibrated Palmer Drought Severity Index (scPDSI; Wells et al., 2004) from the Climate Research Unit (CRU TS v4.07; Harris et al., 2020). For the instrumental comparison, we restricted the window to 1950–2005. The 2005 end date represents the final common year of the reconstructed data (see below). Although the CRU data begin in 1901 across the gridded network, a later start date was chosen as the underlying instrumental station network is poorly replicated during the early 20th century, including northern Mexico (e.g., Stahle et al., 2016a).

2.2. Drought Atlases, Data Assimilation Estimates, and Climate Model Data

Several "drought atlases" based on tree-ring chronologies have been produced since the 1990s (Burnette, 2021; Smerdon et al., 2023). The North American Drought Atlas (NADA) was the first to reconstruct interannual variability of PDSI for a spatial grid, using point-by-point regression (Cook et al., 1999). The NADA was followed by several efforts for other continents and regions, such as eastern Australia-New Zealand (ANZDA; Palmer et al., 2015a), Eurasia (GEDA; Cook et al., 2024), Mexico (MXDA; Stahle et al., 2016a), and South America (SADA; Morales et al., 2020a). These reconstructions represent state-of-the-art estimates of hydroclimatic variability for varying timespans. Here, a common period of 1600–2005 CE is used to test drought agreement among regions that contain a robust teleconnection with equatorial Pacific conditions. Pearson's correlation coefficients were calculated, with degrees of freedom corrected for first-order autocorrelation (Cook & Jacoby, 1977), between the gridded network of reconstructed PDSI and eMEI for 1871–2005. The regional

averages of tree-ring reconstructed PDSI (Figure S1 in Supporting Information S1) were produced for areas that displayed significant correlations ($p < 0.01$) with eMEI over the longest possible overlap (1871–2005).

In addition, PDSI estimates from the Paleo Hydrodynamics Data Assimilation product (PHYDA v2; Steiger et al., 2018) for the four regions identified in the drought atlases were also averaged. The PHYDA utilizes a large network of annually resolved proxies (including tree rings, corals, ice cores, speleothems, and lake sediments), together with climate states from the Community Earth System Model Last Millennium Ensemble (CESM-LME, Landrum et al., 2013; Otto-Bliesner et al., 2016). The data assimilation approach simulates coupled climate and ocean-atmospheric variability, allowing the study of possible drivers of local climatic change. Here, we use the PHYDA ensemble mean. PDSI estimates from nine CESM-LME ensemble members were also analyzed. These time-series span 850–1848 CE and are described by Tejedor et al. (2021). PDSI for both the PHYDA and the CESM-LME output was calculated using the MATLAB code of Jacobi et al. (2013) and is not the self-calibrated version of the index (Dai, 2011), which is used for some of the drought atlases.

2.3. Time Series Analyses

Correlations between gridded PDSI estimates and eMEI were calculated for respective common periods (1871–2005 for the drought atlases and 1871–2000 for the PHYDA). Regionally averaged PDSI estimates from the drought atlases, PHYDA, and CESM-LME members were correlated for 40- to 60-year moving windows. The spectral properties of the eMEI were assessed through calculating periodograms from a discrete Fourier transform (Bloomfield, 2000) and the agreement between regional reconstruction averages across temporal frequencies was tested using bootstrapped coherence analysis (Percival & Constantine, 2006), considering standard Gaussian noise to assess the periodogram similarity significance. Additionally, wavelet coherence (Cook et al., 2016; Grinsted et al., 2004) between pairings of the four regional estimates of PDSI was assessed over the 1600–2005 CE common period. A principal component (PC) analysis (Jolliffe, 2002) was performed on the estimates and PCs were compared to the eMEI, and the 3–7-year waveforms of each PDSI series were extracted through bandpass filtering (Cook et al., 1997).

To assess the statistical significance of changes in reconstructed PDSI agreement across the four regions, the mean regional timeseries were phase-scrambled (Theiler & Prichard, 1996) to produce synthetic versions that retain the individual spectral characteristics and long-term correlations between all pairs of estimates (Cook et al., 2011). As for the drought atlas estimates, moving correlations over 50-year windows were calculated for the six combinations and an average was likewise calculated (representing the mean inter-regional drought relationship). The lowest and highest averaged correlations were retained, and the procedure repeated 10,000 times. Percentiles of a kernel distribution fitted to these extremes were calculated, representing confidence intervals of correlations occurring by chance in a data set of similar internal structure and with similar spectral properties to that of the reconstructed regional PDSI series.

3. Results

3.1. ENSO Imprint on Proxy-Based Drought Estimates, 1871–2005

December-to-March (DJFM) eMEI displays statistically significant correlations ($p < 0.01$) with reconstructed PDSI in several regions of existing drought atlases for 1871–2005 (Figure 1a). Negative correlations are strongest in the Philippines, Thailand, Vietnam, and Myanmar in southeast Asia/SeA), as well as in eastern Australia (EA). Positive correlations are strongest in western Kyrgyzstan and nearby grid points over inner Eurasia (iEU), and for the TexMex region of northcentral Mexico and southwestern United States (TxMx). This spatial pattern does not change considerably when limiting the analysis to 1871–1978 (Figure S2a in Supporting Information S1), representing the earliest end date of tree-ring chronologies used in the drought atlases. The correlating regions are well-established in the literature as being strongly influenced by Pacific SSTs (Dai & Wigley, 2000), and the same relationship is validated when comparing the eMEI time-series to a shorter period of instrumental PDSI data (Figure S2b in Supporting Information S1).

The four regionally averaged PDSI series display extreme individual years and extended periods of drought and pluvial conditions, often independent from each other (Figure S1 in Supporting Information S1). However, the correlations between regions are statistically significant since 1600 CE (Table 1), including that of iEU and TxMx —two regions over 12,000 km apart. The agreement is strongest in the 3–7-year frequency bands (Figure S3 in

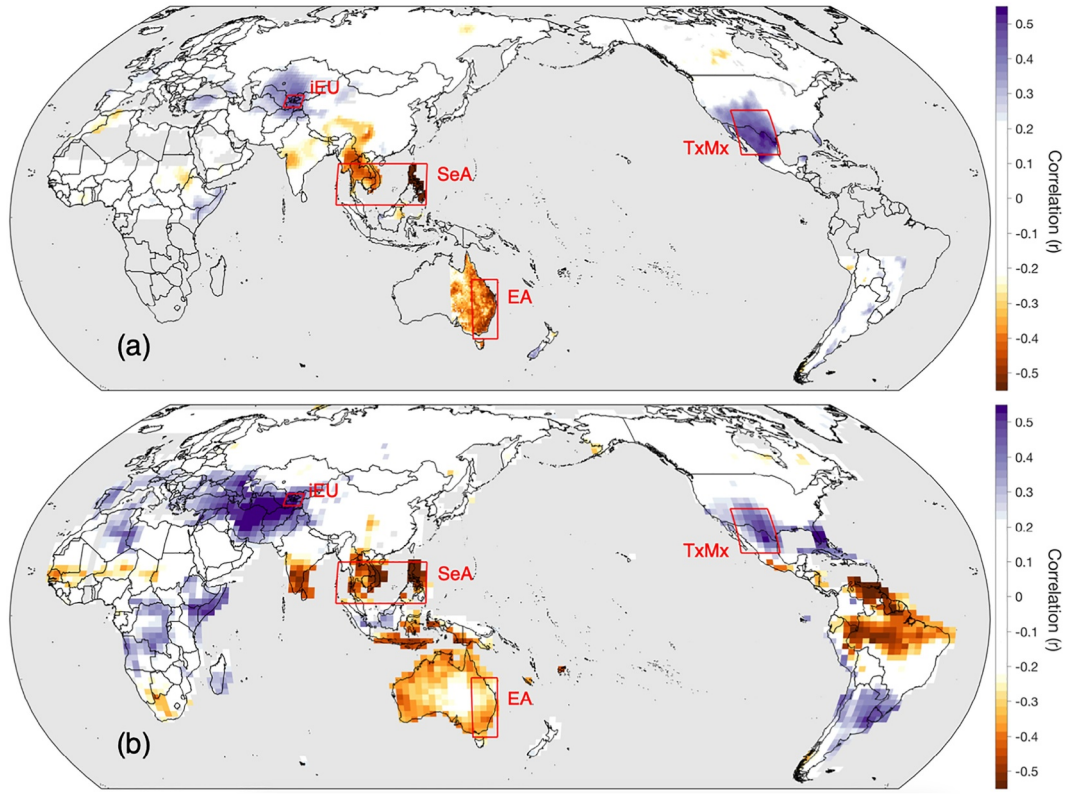

Figure 1. Spatial relationship between ENSO and drought conditions. (a) Correlations between DJFM extended MEI and reconstructed PDSI over the 1871–2005 common period. The four regions representing robust teleconnections are highlighted in red. Gray color indicates space without drought atlas coverage. (b) The same but for PDSI estimates from the PHYDA, over the 1871–2000 common period.

Supporting Information S1), which largely overlaps with the highest power periodicity of the ENSO time-series (An & Jin 2004; Sarachik & Cane, 2010). This result shows that the relationship between regional drought conditions is largely driven by ENSO-like variability, most likely with ENSO as the common driver. Similarly, the first principal component of the four regional PDSI reconstructions displays highly significant ($r = 0.72$, $p < 0.001$) correlation with the instrumental DJFM eMEI from 1871 to 2005 CE (Table S1 in Supporting Information S1).

The correlation patterns are highly similar for the PHYDA over the 1871–2000 CE common period (Figure 1b; Table 1). Over the full study period from 1600 to 2000 CE, the four regions selected based on the drought atlases comparison all display statistically significant correlations ($p < 0.05$) with DJFM eMEI. Statistical significance is reached also for EA, but this may be driven in part by trends in PHYDA PDSI over the past 400 years (Figure S4 in Supporting Information S1). Differences are present outside of these four regions, including various parts of Eurasia as well as notably higher correlations over Florida.

3.2. Temporal Changes in the Relationship Between Regional Soil Moisture

Running correlations between the six possible combinations of regional tree-ring based drought estimates display periods of high and low agreement, of varying magnitudes and timings (Figures 2a–2h). Only for a single period is there a consistent absolute decrease across all combinations—the early 18th century. Running correlations for many of the regions reach their lowest point around this time, including the two pairings that display positive correlations (iEU-TxMx and SeA-EA; Figure 2be). The cooccurring drop is even more distinct when averaging correlations for all regional comparisons (Figure 2g), with the lowest absolute value for the 50-year window present in 1715 CE. The bootstrap simulation of phase-scrambled reconstructions indicates that the drop is statistically significant ($p < 0.01$; Figure S5 in Supporting Information S1). Concurrent with the drop in running correlations is an overall lower agreement between pairs in the 2–8-year band of the wavelet coherence (Figure S6

Table 1
Correlation Matrices for Regional PDSI Estimates for the Full Periods of 1871–2005 and 1600–2005

		1871-2005 (2000)			
Proxy		iEU	SeA	EA	TxMx
	iEU		−0.57	−0.36	0.41
	SeA	−0.34		0.45	−0.39
	EA	−0.27	0.31		−0.28
	TxMx	0.24	−0.32	−0.37	
		1600-2005 (2000)			
Proxy		iEU	SeA	EA	TxMx
	iEU		−0.53	−0.46	0.39
	SeA	−0.29		0.47	−0.36
	EA	−0.21	0.29		−0.35
	TxMx	0.18	−0.27	−0.34	
		850–1848			
CESM-LME		iEU	SeA	EA	TxMx
	iEU		−0.58	−0.27	0.41
	SeA	−0.53		0.31	−0.40
	EA	−0.21	0.22		−0.37
	TxMx	0.31	−0.28	−0.32	

Note. Correlation coefficients for the drought atlases are on the left side. For the PHYDA comparison (in gray; right side), the end date is 2000. Bottom row represents correlations between regional PDSI estimates from nine CESM-LME, with values on the left side representing the lowest magnitude correlations of any ensemble member over 998 years (851–1848 CE) and the right side (gray) the highest magnitude correlations.

in Supporting Information S1). Furthermore, the waveforms for the 3–7-year filtering indicate an out-of-phase period around 1700 (Figure S7 in Supporting Information S1).

Agreement between regional soil moisture estimates in the PHYDA also indicate a drop after 1700 (Figure S8 in Supporting Information S1), but it is not of the largest magnitude over the past 400+ years. Rather, two other departures in the 19th century CE stand out—one in the 1810s and one in the 1880s. An increase then follows, in part driven by sign-shared trend over the second half of the 20th century (Figure S4 in Supporting Information S1), evident in the higher 50-year running correlations toward the present. Conversely, the mean 50-year running correlations display higher agreement for the TxMx comparisons than for the full period (Table 1).

The output from nine CESM-LME ensemble members show the same sign relationship between PDSI for all possible pairings as the PHYDA and drought atlases (Table 1). Magnitudes of correlation are similar to those of the PHYDA. The ensemble members display similar distributions of 50-year running correlations between each other (Figure 3a). However, for the over 8,500 years of modeled data, there are very few instances (four of the nine models have no such recordings) of a breakdown in the average relationship between regions that match the level of the early 1700s proxy-based disruption ($p < 0.005$). The models display high variability in terms of regional and global temperature during the lowest points of inter-regional agreement, but hardly any shared patterns (Figure S9b in Supporting Information S1). Six of the nine models display lower DJFM Niño 3.4 variance in the 50 years prior to the lowest point of agreement (Figure S9a in Supporting Information S1), however, only one falls below the 5th percentile of model variance. Of the nine models, six also show their lowest inter-regional correlation within 20 years following of one of the 10 largest tropical volcanic events (as defined by volumes of volcanic stratospheric sulfur injection; Table S2 in Supporting Information S1; Toohey & Sigl, 2017) of the CESM-LME period (850–1848 CE).

4. Discussion

Reconstructed summer PDSI from tree-ring records in four ENSO-dependent regions display statistically significant relationships over the past 400+ years of reconstructed data. These relationships are also present in instrumental data (Figure S2b in Supporting Information S1). Several thousand kilometers separate the regions and there is a very limited overlap of predictors (i.e., the only instance is a small number of tree-ring chronologies from Java were used in both the ANZDA and the GEDA, Palmer et al., 2015a; Cook et al., 2024). The significant relationship between soil moisture in distant parts of the planet is a distinct example of the importance of the Pacific Ocean on large-scale climate at interannual scales (Cai et al., 2015; Sarachik & Cane, 2010).

The strong teleconnection patterns of regional soil moisture is the underlying mechanism that allows for tree-ring based reconstructions of ENSO (e.g., Stahle et al., 1998; Wilson et al., 2009). Although ENSO is mainly driving climate variability outside of the growing season in the Northern Hemisphere, precipitation in the winter months is a strong driver of summer conditions in regions such as northern Mexico and southwestern US—allowing for tree-ring data to record the teleconnection. The estimates of past ENSO variability from terrestrial proxy records are unavoidably tied to the stability of such teleconnections. Uncertainty in reconstructions of oceanic indices can have a significant impact on pre-instrumental estimates (Batehup et al., 2015; Kipfmueller et al., 2012), and any non-stochastic fluctuations must be understood for robust interpretations to be made. The stability of ocean-atmosphere teleconnections has been studied for some regions (e.g., Coats et al., 2013; Cole & Cook, 1998; Luo et al., 2024; Scholz et al., 2021), but the results presented here indicate a previously unknown episode of non-analogous conditions.

10.1029/2025GL115600

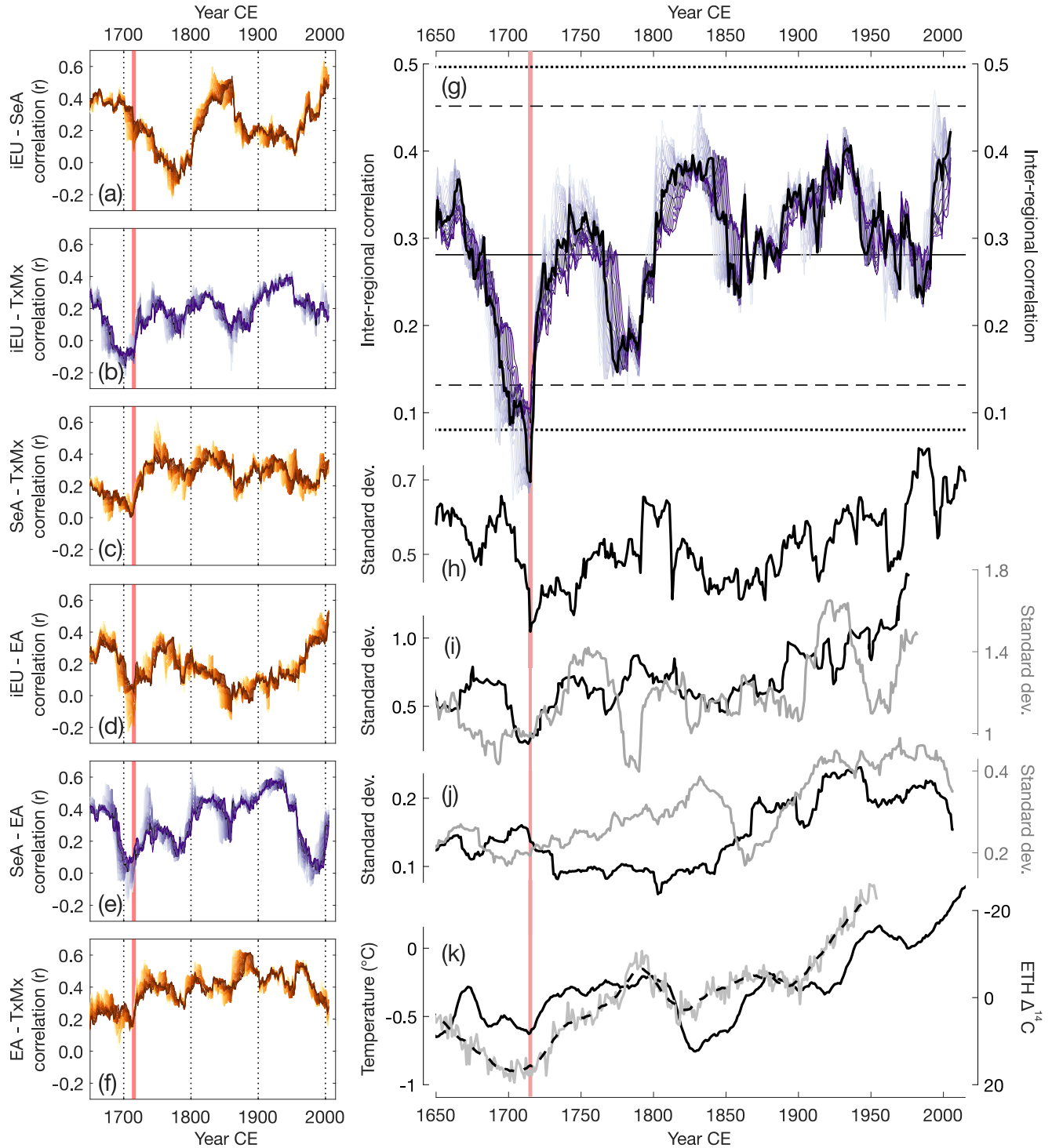

Figure 2. Inter-relationships between regional tree ring-based soil moisture estimates from the drought atlases, and other proxy records. (a–f) Absolute running 40- (light) to 60-year (dark) correlations between reconstructed PDSI of the four ENSO-influenced regions. 50-year correlations in bold black. Purple colors indicate positive correlations, orange colors negative. Red lines highlight the year 1715. (g) Sign-adjusted inter-series correlation between regional PDSI estimates for 40- to 60-year running windows, with the 50-year window highlighted in black. Dotted (dashed) lines indicate the 1/99th (5/95th) percentiles from Monte Carlo-based significance testing for a 50-year window. Solid line indicates the mean of 50-year window for the 406-year period. (h) Running 20-year standard deviations of the Cook & Cane (2024) R15 equatorial Pacific Ocean SST reconstruction. (i) Running 31-year standard deviations of the Wilson et al. (2009) COA-reconstructed ENSO (black) and the Braganza et al. (2009) R5 multi-proxy ENSO reconstruction (gray). (j) Running 31-year standard deviations of warm pool (black) and cold tongue (gray) ENSO reconstructions of Freund et al. (2019). (k) Running 20-year mean of Northern Hemisphere June-August temperature reconstruction of Büntgen et al. (2021; solid black); and interannual (gray) and running 20-year mean (dashed black) of oak ^{14}C measurements associated with sunspot activity (Brehm et al., 2021).

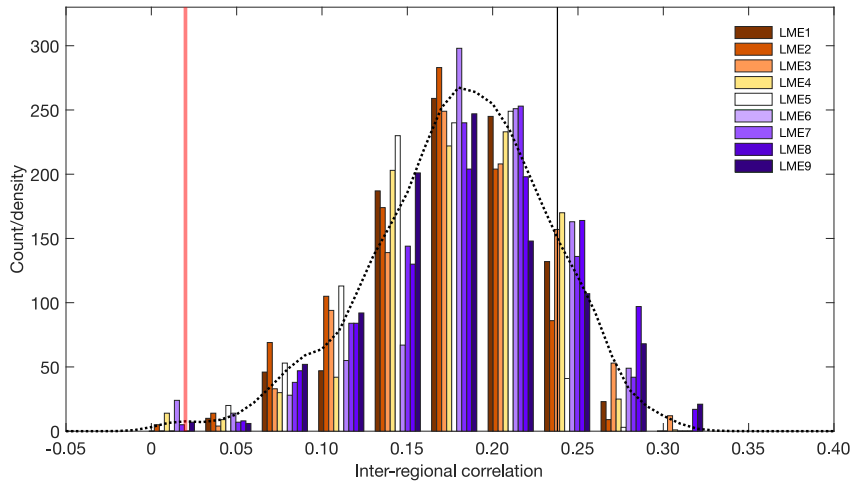

Figure 3. Relationship between regional drought in CESM-LME output. Distributions of running 50-year correlations in nine CESM-LME members for the pre-instrumental period 850–1848 CE, with the dotted black line representing a kernel fit to the data from all members. The vertical lines indicate the mean (black) and lowest (red) levels of inter-regional correlation recorded in the drought atlases around 1700 CE.

4.1. Breakdown of the Relationship Between Soil Moisture in ENSO-Affected Regions

The relationship between individual regional reconstructions varies greatly over the 400-year study period (Figures 2a–2f). Such fluctuations are, of course, expected due to the relatively large non-shared variance. However, the sharp decline in inter-regional correlations recorded in the early 18th century CE is the only statistically significant event since 1600 CE, as estimated from the Monte Carlo simulation based on the long-term relationship between regions. These significance thresholds are supported by CESM-LME model comparisons (Figure 3). Although the PHYDA-based estimates record a small dip in correlation during the same period (Figure S8g in Supporting Information S1), the magnitude of decline is not significant, and other periods display lower values. The skill of the PHYDA estimates must be considered, however, as the EA region only displays similar correlations as the instrumental PDSI during the latter half of the 20th century.

The sharp decrease in correlations in the early 1700s coincides with low variance in the SST reconstruction by Cook & Cane (2024), which displays its lowest running standard deviations around the same time (Figure 2h). Due to a shared pool of tree-ring predictors between (a) the drought atlases and (b) SST reconstruction, it is difficult to assess the independence of cooccurring anomalies. The changing variance in the multi-proxy ENSO reconstruction by Braganza et al. (2009; Figure 2i) also displays agreement with the running averaged drought atlas teleconnections (Figure 2g), not just for the period of breakdown. A coral-based reconstruction from the "center of action" (COA), starting in 1607 CE, displays its lowest point of variance during the early 1700s (Figure 2i; Wilson et al., 2009). However, it should be noted that the COA record is poorly replicated during this period, an issue that is characteristic of the coral record from the central Pacific (Tierney et al., 2015). The Palmyra coral record, which is not continuous and has a gap following the early 18th century, displays a peak in $\delta^{18}O$ around this time—higher than any annual value recorded for the modern corals that start in 1887 (Dee, Cobb, et al., 2020). Freund et al. (2019) presented two spatially separate Pacific SST reconstructions, both showing lower variance during the period of interest (Figure 2j). The multi-proxy reconstruction of ENSO variability by McGregor et al. (2010) displays its lowest point in the early 18th century—although only using tree-ring chronologies from TxMx. The reconstruction of Liu et al. (2024), combining stable isotopes from Pacific-adjacent tree rings and speleothems, also shows a strong decline in variance around 1700. The nine CESM-LME ensemble members do not display statistically significant departures of ENSO variability during the lowest point of inter-regional correlations (Figure S9a in Supporting Information S1). Regardless of associated uncertainties, the overall proxy record for the late 17th and early 18th centuries indicates an anomaly that is unparalleled in the following centuries. Climate models, which may struggle to fully emulate ENSO teleconnections (Weare, 2013), and climate model-driven products fail to capture the extent of this exceptional teleconnection disruption.

4.2. The Role of Temperature and Volcanic Activity in Drought Teleconnections

The disruption of teleconnections herein identified in the drought atlases coincides with what is thought to be one of the coldest periods in the past 1,000 years (Büntgen et al., 2021; Esper et al., 2024) and more so for the study period (Figure 2k). The Maunder minimum—a period of low solar activity (Brehm et al., 2021; Figure 2k) that has been linked to changes in regional and global climate (Shindell et al., 2001)—is generally placed in the mid 1600s with a firm end date of 1715 (Usoskin et al., 2015). Lower temperatures have been suggested to have a negative effect on ENSO variability (Thirumalai et al., 2024) but cooling at a global level would also impact the relative influence of precipitation on drought conditions. With lower evapotranspiration demands, ENSO-driven precipitation variability is arguably less important in producing extreme drought. It is notable that the same relationship, but for the opposite sign, has recently been suggested for the second half of the 7th and first half of the 8th centuries CE. Jiang et al. (2023), using coral data from the South China Sea, propose a distinct phase of increased ENSO activity, which is in part attributed to high solar activity. Conversely, the lower temperatures of the Little Ice Age (LIA) may have enhanced the ENSO teleconnection to North America (Dee, Okumura, et al., 2020)—and the spatial extent of the TxMx-ENSO signal reached its 350-year maximum in the decades around 1700 (Torbenson et al., 2019). Any changes (be it strengthened or weakened) to ENSO influence that is not equal across our regions of interest is likely to negatively affect the inter-regional coherence.

The Maunder solar minimum is concurrent with the height of the LIA, but volcanic eruptions may have played a greater role in the cooling (Owens et al., 2017). A string of large volcanic eruptions occurred within the Pacific Rim in the second half of the 17th century (Gabriel et al., 2025). Four VEI 5 eruptions were recorded between 1663 and 1680 (including Gamkonora in 1673 and Tongkoko in 1680; Briffa et al., 1998; Sigl et al., 2015), in addition to the VEI 6 Long Island eruption of the early 1660s (Blong et al., 2018). The eruption of 1695 of unknown tropical origin (D'Arrigo et al., 2020) qualifies as one of the 10 eruptions compared for the longer model-driven comparison (Table S2 in Supporting Information S1). Although the tropospheric sulfur injections from all these eruptions may not have driven global cooling, Northern Hemisphere temperature reconstructions nonetheless record some of the coolest years of our study period in the 1690s (Briffa et al., 1998; Büntgen et al., 2021).

The influence of volcanism on ENSO has been a frequent topic of paleoclimatic discussion, not always with consensus (Brad Adams et al., 2003; Dee, Cobb, et al., 2020; McGregor et al., 2020; Wilson et al., 2009; Zhu et al., 2022). However, the influence on ENSO is not necessarily the direct interest here—but rather the resulting strength of teleconnections between regions due to ENSO. The PHYDA displays the strongest negative anomalies in regional agreement following some of the largest eruptions of the 1600–2000 CE study period: Tambora in 1815 and Krakatau in 1884 (Figure S8 in Supporting Information S1). Previous analyses of the PHYDA have shown that the strongest response of winter PDSI to volcanic forcings is present over inner Eurasia (Tejedor et al., 2021). However, the change recorded in the PHYDA is not statistically significant and the relationship between regional summer PDSI in the drought atlases does not display any disruption around these 19th century eruptions. Thus, we do not attribute the disruption of teleconnections to any specific forcing beyond noting the apparent coincidence of concurrent cooling.

4.3. Implications and Directions for Future Work

Although both proxy-only and data assimilation approaches have various limitations associated, data assimilation products and climate models are becoming increasingly important for our understanding of past climate variability (Cai et al., 2021; Zhu et al., 2022). Although neither the CESM-LME nor the PHYDA ensembles reproduce a breakdown of comparable magnitude, PHYDA's assimilation of proxy data nevertheless records a negative departure coincident with that of the drought atlases (albeit without reaching statistical significance). This alignment underscores the crucial role of proxy records in constraining reconstruction variance: by injecting real-world signals into the model prior, data assimilation products like PHYDA can reveal transient climate anomalies that purely model-driven approaches may underestimate or entirely miss. Further investigation, for example, of other data assimilation products, may provide additional insights on potential drivers and model restraints. Climate models already have difficulties in capturing observational trends (Jiang et al., 2024; Seager et al., 2019), and the varying response of ENSO to volcanic forcings may partly be caused by initial stage conditions (Predybaylo et al., 2020). It is worth noting that many of the CESM-LME ensemble members show the lowest inter-regional correlation following major eruptions (Table S2 in Supporting Information S1).

Our results also highlight the need for proxy records in regions impacted by ENSO variability but that are not represented in the analysis, such as the Amazon basin and eastern and southern Africa (Figure S2b in Supporting Information S1). The analysis presented here is limited to four regions for which we have robust reconstructions of hydroclimatic variability over the past 400 years. Analyses of tree rings in northern Brazil suggest that a strong relationship does exist with TxMx tree-ring chronologies (and sign-aligned with the ENSO teleconnection), but the tropical records do not start until the mid 1700s (Stahle et al., 2020). Increased ENSO variability has also been suggested to synchronize tree growth outside of these traditional ENSO-influenced regions, such as in south-eastern China (Su et al., 2024). Finally, many of the tree-ring records in ENSO teleconnection regions end in the early 2000s or earlier (Cook & Cane, 2024) and we therefore miss the critical years of recent warming that may be key for our understanding of this phenomenon.

5. Conclusions

We describe an unusual breakdown in the teleconnection of drought conditions between remote ENSO-related regions in Asia, Eastern Australia, and North America during the early 18th century CE. Although the relationship between tree-ring based PDSI reconstructions for any regional pairing varied greatly over the past 400+ years, the disruption of combined correlation pairs following 1700 is the only statistically significant event and represents a considerable departure from the modern teleconnection pattern captured by a dense network of meteorological stations. Although temporal coincidence with the well-known Maunder solar minimum is notable, we do not suggest causation. What we describe as a disruption event could, in fact, be part of natural variability. The period may, nonetheless, be of interest for climate model studies as it represents a mechanistically puzzling ocean-atmosphere dynamic previously undetected. Future work should attempt to attribute the breakdown to physical processes and explore other periods of potential change, including recent decades.

Conflict of Interest

The authors declare no conflicts of interest relevant to this study.

Data Availability Statement

The PHYDA ensemble mean, as well as individual runs, are available through Steiger (2018). The drought atlases are available through NOAA Paleoclimatology (Cook et al., 2010; Morales et al., 2020b; Palmer et al., 2015b; Stahle et al., 2016b). CESM-LME data sets used are available through CCSM (2024).

Acknowledgments
MCAT, JE and UB acknowledge support from ERC (Advanced Grant #882727 and Synergy Grant #101118880), and with MT the Czech Science Foundation (#23-08049S) and Ministry of Education, Youth and Sports of the Czech Republic (CZ.02.01.01/00/22_008/0004635). DWS was supported by the National Science Foundation (Grant AGS-2201243). ET is supported by the Comunidad de Madrid program Atracción Talento "César Nombela" Grant 2023-T1/ECO-29118. Open Access funding enabled and organized by Projekt DEAL.

References

An, S.-I., & Jin, F.-F. (2004). Nonlinearity and asymmetry of ENSO. *Journal of Climate*, *17*(12), 2399–2412. https://doi.org/10.1175/1520-0442(2004)017<2399:NAAOE>2.0.CO;2

Batehup, R., McGregor, S., & Gallant, A. J. E. (2015). The influence of non-stationary teleconnections on paleoclimate reconstructions of ENSO variance using a pseudoproxy framework. *Climate of the Past*, *11*(12), 1733–1749. https://doi.org/10.5194/cp-11-1733-2015

Blong, R., Fallon, S., Wood, R., McKee, C., Chen, K., Magill, C., & Barter, P. (2018). Significance and timing of the mid-17th-century eruption of Long Island, Papua New Guinea. *The Holocene*, *28*(4), 529–544. https://doi.org/10.1177/0959683617735589

Bloomfield, P. (2000). *Fourier analysis of time series: An introduction* (2nd ed., p. 261). John Wiley & Sons.

Brad Adams, J., Mann, M. E., & Ammann, C. M. (2003). Proxy evidence for an El Niño-like response to volcanic forcing. *Nature*, *426*(6964), 274–278. https://doi.org/10.1038/nature02101

Braganza, K., Gergis, J. L., Power, S. B., Risbey, J. S., & Fowler, A. M. (2009). A multiproxy index of the El Niño- Southern Oscillation, A.D. 1525-1982. *Journal of Geophysical Research*, *114*(D5). https://doi.org/10.1029/2008JD010896

Brehm, N., Bayliss, A., Christl, M., Synal, H.-A., Adolphi, F., Beer, J., et al. (2021). Eleven-year solar cycles over the last millennium revealed by radiocarbon in tree rings. *Nature Geoscience*, *14*(1), 10–15. https://doi.org/10.1038/s41561-020-00674-0

Briffa, K. R., Jones, P. D., Schweingruber, F. H., & Osborn, T. J. (1998). Influence of volcanic eruptions on Northern Hemisphere summer temperature over the past 600 years. *Nature*, *393*(6684), 450–455. https://doi.org/10.1038/30943

Büntgen, U., Allen, K., Anchukaitis, K. J., Arseneault, D., Boucher, E., Bräuning, A., et al. (2021). The influence of decision-making in tree ring-based climate reconstructions. *Nature Communications*, *12*(1), 3411. https://doi.org/10.1038/s41467-021-23627-6

Burnette, D. J. (2021). The tree-ring drought atlas portal: Gridded drought reconstructions for the past 500– 2,000 years. *Bulletin of the American Meteorological Society*, *102*(10), 953–956. https://doi.org/10.1175/BAMS-D-20-0142.1

Cai, W., McPhaden, M. J., Grimm, A. M., Rodrigues, R. R., Taschetto, A. S., Garreaud, R. D., et al. (2020). Climate impacts of the El Niño-Southern Oscillation on South America. *Nature Reviews Earth & Environment*, *1*(4), 215–231. https://doi.org/10.1038/s43017-020-0040-3

Cai, W., Santoso, A., Collins, M., Dewitte, B., Karamperidou, C., Kug, J.-S., et al. (2021). Changing El Niño-Southern Oscillation in a warming climate. *Nature Reviews Earth & Environment*, *2*(9), 628–644. https://doi.org/10.1038/s43017-021-00199-z

Cai, W., Santoso, A., Wang, G., Yeh, S.-W., An, S.-I., Cobb, K. M., et al. (2015). ENSO and greenhouse warming. *Nature Climate Change*, *5*(9), 849–859. https://doi.org/10.1038/nclimate2743

Cai, W., Wang, G., Dewitte, B., Wu, L., Santoso, A., Takahashi, K., et al. (2018). Increased variability of eastern Pacific El Niño under greenhouse warming. *Nature*, *564*(7735), 201–206. https://doi.org/10.1038/s41586-018-0776-9

CCSM. (2024). CESM1 last millennial ensemble [Dataset]. Retrieved from https://www.earthsystemgrid.org/dataset/ucar.cgd.ccsm4.cesmLME.html

Coats, S., Smerdon, J. E., Cook, B. I., & Seager, R. (2013). Stationarity of the tropical Pacific teleconnection to North America in CMIP5/PMIP3 model simulations. *Geophysical Research Letters*, *40*(18), 4927–4932. https://doi.org/10.1002/grl.50938

Cobb, K. M., Charles, C. D., Cheng, H., & Edwards, R. L. (2003). El Niño/Southern Oscillation and tropical Pacific climate during the last millennium. *Nature*, *424*(6946), 271–276. https://doi.org/10.1038/nature01779

Cobb, K. M., Charles, C. D., & Hunter, D. E. (2001). A central tropical Pacific coral demonstrates Pacific, Indian, and Atlantic decadal climate connections. *Geophysical Research Letters*, *28*(11), 2209–2212. https://doi.org/10.1029/2001GL012919

Cole, J. E., & Cook, E. R. (1998). The changing relationship between ENSO variability and moisture balance in the continental United States. *Geophysical Research Letters*, *25*(24), 4529–4532. https://doi.org/10.1029/1998GL900145

Cole, J. E., Fairbanks, R. G., & Shen, G. T. (1993). Recent variability in the Southern Oscillation: Results from a Tarawa Atoll coral. *Science*, *260*(5115), 1790–1793. https://doi.org/10.1126/science.260.5115.1790

Cook, B. I., Anchukaitis, K. J., Touchan, R., Meko, D. M., & Cook, E. R. (2016). Spatiotemporal drought variability in the Mediterranean over the last 900 years. *Journal of Geophysical Research – Atmospheres*, *121*(5), 2060–2074. https://doi.org/10.1029/2018JD029323

Cook, B. I., Cook, E. R., Anchukaitis, K. J., Seager, R., & Miller, R. L. (2011). Forced and unforced variability of twentieth century North American droughts and pluvials. *Climate Dynamics*, *37*(5–6), 1097–1110. https://doi.org/10.1007/s00382-010-0897-9

Cook, B. I., Cook, E. R., Anchukaitis, K. J., & Singh, D. (2024). Characterizing the 2010 Russian heat wave – Pakistan flood concurrent extreme over the last millennium using the Great Eurasian Drought Atlas. *Journal of Climate*, *37*(17), 4389–4401. https://doi.org/10.1175/JCLI-D-23-0773.1

Cook, E. R., & Cane, M. A. (2024). Tree rings reveal ENSO in the last millennium. *Geophysical Research Letters*, *51*(19). https://doi.org/10.1029/2024GL109759

Cook, E. R., & Jacoby, G. C. (1977). Tree-ring-drought relationships in the Hudson Valley, New York. *Science*, *198*(4315), 399–401. https://doi.org/10.1126/science.198.4315.399

Cook, E. R., Meko, D. M., & Stockton, C. W. (1997). A new assessment of possible solar and lunar forcing of the bidecadal drought rhythm in the western United States. *Journal of Climate*, *10*(6), 1343–1356. https://doi.org/10.1175/1520-0442(1997)010<1343:ANAOPS>2.0.CO;2

Cook, E. R., Meko, D. M., Stahle, D. W., & Cleaveland, M. K. (1999). Drought reconstructions for the continental United States. *Journal of Climate*, *12*(4), 1145–1162. https://doi.org/10.1175/1520-0442(1999)012%3C1145:DRFTCU%3E2.0.CO;2

Cook, E. R., Seager, R., Heim, R. R., Vose, R. S., Herweijer, C., & Woodhouse, C. A. (2010). The 'living blended drought atlas (LBDA)' North American drought reconstruction for the last 2000 years [Dataset]. *NOAA Paleoclimatology*. https://doi.org/10.25921/xyj1-3836

Dai, A. (2011). Characteristics and trends in various forms of the palmer drought severity index during 1900- 2008. *Journal of Geophysical Research*, *116*(D12), D12115. https://doi.org/10.1029/2010JD015541

Dai, A., & Wigley, T. M. L. (2000). Global patterns of ENSO-induced precipitation. *Geophysical Research Letters*, *27*(9), 1283–1286. https://doi.org/10.1029/1999GL011140

D'Arrigo, R., Cook, E. R., Wilson, R. J., Allan, R., & Mann, M. E. (2005). On the variability of ENSO over the past six centuries. *Geophysical Research Letters*, *32*(3). https://doi.org/10.1029/2004GL022055

D'Arrigo, R., Klinger, P., Newfield, T., Rydval, M., & Wilson, R. (2020). Complexity in crisis: The volcanic cold pulse of the 1690s and the consequences of Scotland's failure to cope. *Journal of Volcanology and Geothermal Research*, *389*, 106746. https://doi.org/10.1016/j.volgeores.2019.106746

Dee, S., Okumura, Y., Stevenson, S., & Di Nezio, P. (2020). Enhanced North American ENSO teleconnections during the Little Ice Age revealed by paleoclimate data assimilation. *Geophysical Research Letters*, *47*(15). https://doi.org/10.1029/2020GL087504

Dee, S. G., Cobb, K. M., Emile-Geay, J., Ault, T. R., Edwards, R. L., Cheng, H., & Charles, C. D. (2020). No consistent ENSO response to volcanic forcing over the last millennium. *Science*, *367*(6485), 1477–1481. https://doi.org/10.1126/science.aax2000

Esper, J., Torbenson, M. C. A., & Büntgen, U. (2024). 2023 summer warmth unparalleled over the past 2,000 years. *Nature*, *631*(8019), 94–97. https://doi.org/10.1038/s41586-024-07512-y

Freund, M. B., Henley, B. J., Karoly, D. J., McGregor, H. V., Abram, N. J., & Dommenget, D. (2019). Higher frequency of central Pacific El Niño events in recent decades relative to past centuries. *Nature Geoscience*, *12*(6), 450–455. https://doi.org/10.1038/s41561-019-0353-3

Gabriel, I., Innes, H. M., Abbott, P. M., Franke, J., Behrens, M., Chellman, N. J., et al. (2025). Constraining the timing and climate forcing of the Long Island (Papua New Guinea) and Tarume (Japan) eruptions and other 17th century volcanic eruptions. *Journal of Volcanology and Geothermal Research*, *464*, 108346. https://doi.org/10.1016/j.jvolgeores.2025.108346

Gebre, T., Abraha, Z., Zenebe, A., & Zeweld, W. (2023). Precipitation variability and its teleconnection with the global SST and ENSO indices in the food-insecure rural areas of Tigray. *Theoretical and Applied Climatology*, *155*(3), 1699–1711. https://doi.org/10.1007/s00704-023-04717-5

Grinsted, A., Moore, J. C., & Jevrejeva, S. (2004). Application of the cross wavelet transform and wavelet coherence to geophysical time series. *Nonlinear Processes in Geophysics*, *11*(5/6), 561–566. https://doi.org/10.5194/npg-11-561-2004

Harris, I., Osborn, T. J., Jones, P., & Lister, D. (2020). Version 4 of the CRU TS monthly high-resolution gridded multivariate climate dataset. *Scientific Data*, *7*(1), 109. https://doi.org/10.1038/s41597-020-0453-3

Heede, U. K., & Fedorov, A. V. (2023). Towards understanding the robust strengthening of ENSO and more frequent extreme El Niño events in CMIP6 global warming simulations. *Climate Dynamics*, *61*, 3047–3060. https://doi.org/10.1007/s00382-023-06856-x

IPCC. (2021). In V. Masson-Delmotte, P. Zhai, A. Pirani, S. L. Connors, C. Péan, S. Berger, et al. (Eds.), *Climate change 2021: The physical science basis. Contribution of working Group I to the sixth assessment report of the intergovernmental panel on climate change*. Cambridge University Press. https://doi.org/10.1017/9781009157896

Jacobi, J., Perrone, D., Duncan, L. L., & Hornberger, G. (2013). A tool for calculating the Palmer drought indices. *Water Resources Research*, *49*(9), 6086–6089. https://doi.org/10.1002/wrcr.20342

Jiang, F., Seager, R., & Cane, M. A. (2024). A climate change signal in the tropical Pacific emerges from decadal variability. *Nature Communications*, *15*(1), 8291. https://doi.org/10.1038/s41467-024-52731-6

Jiang, L., Yu, K., Tao, S., Li, Y., & Wang, S. (2023). Abrupt increase in ENSO variability at 700 CE triggered by solar activity. *Journal of Geophysical Research: Oceans*, *128*(1). https://doi.org/10.1029/2022JC019278

Jolliffe, I. T. (2002). *Principal component analysis*. Springer.

Kipfmueller, K. F., Larson, E. R., & George, S. S. (2012). Does proxy uncertainty affect the relations inferred between the Pacific Decadal Oscillation and wildfire activity in the western United States? *Geophysical Research Letters*, *39*(4). https://doi.org/10.1029/2011GL050645

Landrum, L., Otto-Bliesner, B. L., Wahl, E. R., Conley, A., Lawrence, P. J., Rosenbloom, N., & Teng, H. (2013). Last millennium climate and its variability in CCSM4. *Journal of Climate*, *26*(4), 1085–1111. https://doi.org/10.1175/JCLI-D-11-00326.1

Li, J., Xie, S.-P., Cook, E. R., Morales, M. S., Christie, D. A., Johnson, N. C., et al. (2013). El Niño modulations over the past seven centuries. *Nature Climate Change*, *3*(9), 822–826. https://doi.org/10.1038/nclimate1936

Liguori, G., McGregor, S., Singh, M., Arblaster, J., & Di Lorenzo, E. (2022). Revisiting ENSO and IOD contributions to Australian precipitation. *Geophysical Research Letters*, *49*(1). https://doi.org/10.1029/2021GL094295

Liu, Y., Man, W., Zhou, T., & Zuo, M. (2024). Global multiproxy ENSO reconstruction over the past millennium. *Journal of Geophysical Research – Atmospheres*, *129*(10). https://doi.org/10.10129/2023JD040491

Lough, J. M., & Fritts, H. C. (1985). The Southern Oscillation and tree rings: 1600–1961. *Journal of Applied Meteorology and Climatology*. *24*, 952–966. https://doi.org/10.1175/1520-0450(1985)024<0952:TSOATR>2.0.CO;2

Luo, X., Dee, S., Okumura, Y., & Parsons, L. (2024). Nonstationary teleconnections over North America revealed in paleoclimate data assimilation reconstructions spanning the last millennium. *Journal of Geophysical Research: Atmospheres*, *129*(22). https://doi.org/10.1029/2024JD041150

McGregor, G. R., & Ebi, K. (2018). El Niño Southern Oscillation (ENSO) and health: An overview for climate and health researchers. *Atmosphere*, *9*(7), 282. https://doi.org/10.3390/atmos9070282

McGregor, S., Khodri, M., Maher, N., Ohba, M., Pausata, F. S. R., & Stevenson, S. (2020). The effect of strong volcanic eruptions on ENSO. In M. J. McPhaden, A. Santoso, & W. Cai (Eds.), *El Niño Southern Oscillation in a changing climate*, *Geophysical Monograph Series*. AGU.

McGregor, S., Timmermann, A., & Timm, O. (2010). A unified proxy for ENSO and PDO variability since 1650. *Climate of the Past*, *6*, 1–17. https://doi.org/10.5194/cp-6-1-2010

Meque, A., & Abiodun, B. J. (2015). Simulating the link between ENSO and summer drought in Southern Africa using regional climate models. *Climate Dynamics*, *44*(7–8), 1881–1900. https://doi.org/10.1007/s00382-014-2143-3

Morales, M. S., Cook, E. R., Barichivich, J., Christie, D. A., Villalba, R., LeQuesne, C., et al. (2020a). Six hundred years of South American tree rings reveal an increase in severe hydroclimatic events since mid-20th century. *Proceedings of the National Academy of Sciences of the United States of America*, *117*(29), 16816–16823. https://doi.org/10.1073/pnas.2002411117

Morales, M. S., Cook, E. R., Barichivich, J., Christie, D. A., Villalba, R., LeQuesne, C., et al. (2020b). South American drought atlas (SADA) for south central South America, 1400-2000 C.E., Austral summer PDSI reconstructions [Dataset]. *NOAA Paleoclimatology*. https://doi.org/10.25921/b1ps-rw37

Nguyen-Thanh, H., Ngo-Duc, T., & Herrmann, M. (2023). The distinct impacts of the two types of ENSO on rainfall variability over Southeast Asia. *Climate Dynamics*, *61*(5–6), 2155–2172. https://doi.org/10.1007/s00382-023-06673-2

Otto-Bliesner, B. L., Brady, E. C., Fasullo, J., Jahn, A., Landrum, L., Stevenson, S., et al. (2016). Climate variability and change since 850 CE: An ensemble approach with the Community Earth System Model. *Bulletin of the American Meteorological Society*, *97*(5), 735–754. https://doi.org/10.1175/BAMS-D-14-00233.1

Owens, M. J., Lockwood, M., Hawkins, E., Usoskin, I., Jones, G. S., Barnard, L., et al. (2017). The Maunder minimum and the little ice Age: An update from recent reconstructions and climate simulations. *Journal of Space Weather and Space Climate*, *7*, A33. https://doi.org/10.1051/swsc/2017034

Palmer, J. G., Cook, E. R., Turney, C. S. M., Allen, K., Fenwick, P., Cook, B. I., et al. (2015a). Drought variability in eastern Australia and New Zealand summer drought atlas (ANZDA, CE 1500-2012) modulated by the Interdecadal Pacific Oscillation. *Environmental Research Letters*, *10*(12), 124002. https://doi.org/10.1088/1748-9326/10/12/124002

Palmer, J. G., Cook, E. R., Turney, C. S. M., Allen, K. J., Fenwick, P., Cook, B. I., et al. (2015b). Eastern Australia and New Zealand Drought Atlas (ANZDA) [Dataset]. *NOAA Paleoclimatology*. https://doi.org/10.25921/7qpw-x384

Percival, D. B., & Constantine, W. L. B. (2006). Exact simulation of Gaussian time series from nonparametric spectral estimates with application to bootstrapping. *Statistics and Computing*, *16*(1), 25–35. https://doi.org/10.1007/s11222-006-5198-0

Predybaylo, E., Stenchikov, G., Wittenberg, A. T., & Osipov, S. (2020). El Niño/Southern Oscillation response to low-latitude volcanic eruptions depends on ocean pre-conditions and eruption timing. *Communications Earth & Environment*, *1*, 12. https://doi.org/10.1038/s43247-020-0013-y

Raghuraman, S. P., Soden, B., Clement, A., Vecchi, G., Menemenlis, S., & Yang, W. (2024). The 2023 global warming spike was driven by the El Niño-Southern Oscillation. *Atmospheric Chemistry and Physics*, *24*(19), 11275–11283. https://doi.org/10.5194/acp-24-11275-2024

Rosenthal, Y., & Broccoli, A. J. (2004). In search of Paleo-ENSO. *Science*, *304*(5668), 219–221. https://doi.org/10.1126/science.1095435

Sarachik, E., & Cane, M. (2010). *The El Niño-Southern Oscillation phenomenon*. Cambridge University Press.

Scholz, S. R., Seager, R., Ting, M., Kushnir, Y., Smerdon, J. E., Cook, B. I., et al. (2021). Changing hydroclimate dynamics and the 19th and 20th century wetting trend in the English Channel region of northwest Europe. *Climate Dynamics*, *58*(5–6), 1539–1553. https://doi.org/10.1007/s00382-021-05977-5

Scroxton, N., & McKay, N. (2024). The hunt for Holocene abrupt climate change. *PLOS Climate*, *3*(12), e0000547. https://doi.org/10.1371/journal.pclm.0000547

Seager, R., Cane, M., Henderson, N., Lee, D.-E., Abernathey, R., & Zhang, H. (2019). Strengthening tropical Pacific zonal sea surface temperature gradient consistent with rising greenhouse gases. *Nature Climate Change*, *9*(7), 517–522. https://doi.org/10.1038/s41558-019-0505-x

Shindell, D. T., Schmidt, G. A., Mann, M. E., Rind, D., & Waple, A. (2001). Solar forcing of regional climate change during the Maunder minimum. *Science*, *294*(5549), 2149–2152. https://doi.org/10.1126/science.1064363

Sigl, M., Winstrup, M., McConnell, J. R., Welten, K. C., Plunkett, G., Ludlow, F., et al. (2015). Timing and climate forcing of volcanic eruptions for the past 2,500 years. *Nature*, *523*(7562), 543–562. https://doi.org/10.1038/nature14565

Singh, J., Ashfaq, M., Skinner, C. B., Anderson, W. B., Mishra, V., & Singh, D. (2022). Enhanced risk of concurrent regional droughts with increased ENSO variability and warming. *Nature Climate Change*, *12*(2), 163–170. https://doi.org/10.1038/s41558-021-01276-3

Smerdon, J. E., Cook, E. R., & Steiger, N. J. (2023). The historical development of large-scale paleoclimate field reconstructions over the Common Era. *Reviews of Geophysics*, *61*(4), e2022RG000782. https://doi.org/10.1029/2022RG000782

Stagge, J. H., Torbenson, M. C. A., Sung, K., Phillips, B., & Kingston, D. G. (2023). Orographic amplification of El Niño teleconnections on winter precipitation across the intermountain west of North America. *Nature Water*, *1*(12), 1016–1026. https://doi.org/10.1038/s44221-023-00163-9

Stahle, D. W., & Cleaveland, M. K. (1993). Southern Oscillation extremes reconstructed from tree-rings of the Sierra Madre Occidental and the southern Great Plains. *Journal of Climate*, *6*(1), 129–140. https://doi.org/10.1175/1520-0442(1993)006<0129:SOERFT>2.0.CO;2

Stahle, D. W., Cook, E. R., Burnette, D. J., Villanueva, J., Cerano, J., Burns, J. N., et al. (2016a). The Mexican Drought Atlas: Tree-ring reconstructions of the soil moisture balance during the late pre-Hispanic, colonial, and moder eras. *Quaternary Science Reviews*, *149*, 34–60. https://doi.org/10.1016/j.quascirev.2016.06.018

Stahle, D. W., Cook, E. R., Burnette, D. J., Villanueva, J., Cerano, J., Burns, J. N., et al. (2016b). Mexican Drought Atlas (MXDA) 600 Year scPDSI reconstructions [Dataset]. *NOAA Paleoclimatology*. https://doi.org/10.25921/8frg-zb33

Stahle, D. W., D'Arrigo, R. D., Krusic, P. J., Cleaveland, M. K., Cook, E. R., Allan, R. J., et al. (1998). Experimental dendroclimatic reconstruction of the Southern Oscillation. *Bulletin of the American Meteorological Association*, *79*(10), 2137–2152. https://doi.org/10.1175/1520-0477(1998)079<2137:EDROTS>2.0.CO;2

Stahle, D. W., Torbenson, M. C. A., Howard, I. M., Granato-Souza, D., Barbosa, A. C., Feng, S., et al. (2020). Pan American interactions of Amazon precipitation, streamflow, and tree growth extremes. *Environmental Research Letters*, *15*(10), 104092. https://doi.org/10.1088/1748-9326/ababc6

Steiger, N. J. (2018). Paleo hydrodynamics data assimilation product (PHYDA) [Dataset]. *Zenodo*. https://doi.org/10.5281/zenodo.1198817

Steiger, N. J., Smerdon, J. E., Cook, E. R., & Cook, B. I. (2018). A reconstruction of global hydroclimate and dynamical variables over the Common Era. *Scientific Data*, *5*(1), 180086. https://doi.org/10.1038/sdata.2018.86

Su, J., Gou, X., Hille Ris Lambers, J., Zhang, D. D., Zheng, W., Xie, M., & Manzanedo, R. D. (2024). Increasing ENSO variability synchronizes tree growth in subtropical forests. *Agricultural and Forest Meteorology*, *345*, 109830. https://doi.org/10.1016/j.agrformet.2023.109830

Tang, S., Qiao, S., Wang, B., Liu, F., Zhu, X., Feng, T., et al. (2024). Recent changes in ENSO's impacts on the summertime circumglobal teleconnection and mid-latitude extremes. *Nature Communications*, *16*(1), 646. https://doi.org/10.1038/s41467-025-55925-8

Tejedor, E., Steiger, N. J., Smerdon, J. E., Serrano-Notivoli, R., & Vuille, M. (2021). Global hydroclimatic response to tropical volcanic eruptions over the last millennium. *Proceedings of the National Academy of Sciences*, *118*(12), e2019145118. https://doi.org/10.1073/pnas.2019145118

Theiler, J., & Prichard, D. (1996). Constrained-realization Monte-Carlo method for hypothesis testing. *Physica D: Nonlinear Phenomena*, *94*(4), 221–235. https://doi.org/10.1016/0167-2789(96)00050-4

Thirumalai, K., DiNezio, P. N., Partin, J. W., Liu, D., Costa, K., & Jacobel, A. (2024). Future increase in extreme El Niño supported by past glacial changes. *Nature*, *634*(8033), 374–380. https://doi.org/10.1038/s41586-024-07984-y

Tierney, J. E., Abram, N. J., Anchukaitis, K. J., Evans, M. N., Giry, C., Kilbourne, K. H., et al. (2015). Tropical sea surface temperatures for the past four centuries reconstructed from coral archives. *Paleoceanography*, *30*(3), 226–252. https://doi.org/10.1002/2014PA002717

Toohey, M., & Sigl, M. (2017). Volcanic stratospheric sulfur injections and aerosol optical depth from 500 BCE to 1900 CE. *Earth System Science Data*, *9*(2), 809–831. https://doi.org/10.5194/essd-9-809-2017

Torbenson, M. C. A., Stahle, D. W., Howard, I. M., Burnette, D. J., Villanueva-Díaz, J., Cook, E. R., & Griffin, D. (2019). Multidecadal modulation of the ENSO teleconnection to precipitation and tree growth over subtropical North America. *Paleoceanography and Paleoclimatology*, *34*(5), 886–900. https://doi.org/10.1029/2018PA003510

Usoskin, I. G., Arlt, R., Asvestari, E., Hawkins, E., Käpylä, M., Kovaltsov, G. A., et al. (2015). The Maunder minimum (1645-1715) was indeed a grand minimum: A reassessment of multiple datasets. *Astronomy & Astrophysics*, *581*, A95. https://doi.org/10.1051/0004-6361/201526652

Weare, B. C. (2013). El Niño teleconnections in CMIP5 models. *Climate Dynamics*, *41*(7–8), 2165–2177. https://doi.org/10.1007/s00382-012-1537-3

Wells, N. S., Goddard, S., & Hayes, M. J. (2004). A self-calibrating palmer drought severity index. *Journal of Climate*, *17*(12), 2335–2351. https://doi.org/10.1175/1520-0442(2004)017<2335:ASPDSI>2.0.CO;2

Wilson, R., Cook, R. E., D'Arrigo, R., Riedwyl, N., Evans, M. N., Tudhope, A., & Allan, R. (2009). Reconstructing ENSO: The influence of method, proxy data, climate forcing and teleconnections. *Journal of Quaternary Science*, *25*(1), 62–78. https://doi.org/10.1002/jqs.1297

Wittenberg, A. T. (2009). Are historical records sufficient to constrain ENSO simulations? *Geophysical Research Letters*, *36*(12), L12702. https://doi.org/10.1029/2009GL038710

Wolter, K., & Timlin, M. S. (2011). El Niño/Southern Oscillation behaviour since 1871 as diagnosed in an extended multivariate ENSO index (MEI.ext). *International Journal of Climatology*, *37*, 1074–1087. https://doi.org/10.1002/joc.2336

Yeh, S. W., Cai, W., Min, S.-K., McPhaden, M. J., Dommenget, D., Dewitte, B., et al. (2018). ENSO atmospheric teleconnections and their response to greenhouse gas forcing. *Reviews of Geophysics*, *56*(1), 185–206. https://doi.org/10.1002/2017RG000568

Zhu, F., Emile-Geay, J., Anchukaitis, K. J., Hakim, G. J., Wittenberg, A. T., Morales, M. S., et al. (2022). A re-appraisal of the ENSO response to volcanism with paleoclimate data assimilation. *Nature Communications*, *13*(1), 747. https://doi.org/10.1038/s41467-022-28210-1